The Comparison of Two Types of Boundary Conditions for the Active Electrode in Simulation of Ionic Wind

Kostin P.A., Poluektova K.D., Elagin I.A., Markovskii P.Y.
p.kostin@2014.spbu.ru

Abstract

The paper deals with computer simulation of ionic wind in the needle-plane electrode system with the positive polarity of the active electrode. Complicated processes in the corona sheath are substituted with two types of boundary conditions at the anode. The first method utilizes an approach, where the density of the flow of positive ions is set at the active electrode as the linear function of the electric field strength. Defining the function requires experimental values of ignition voltage of corona discharge measured for each electrode in the system under simulation. The second method uses a more complicated boundary condition for the ion flow, which bases on calculation of the number of ionization collisions near the anode surface. The advantage of the model is that it requires no experimental input data at a change of the electrode configuration. To verify the performance of the models, the structure of ionic wind in the needle-plate system was studied experimentally. The I-V curves of corona discharge were measured over a wide range of voltages. Air velocity distributions in the inter-electrode gap were obtained by the Particle Image Velocimetry method. Distributions of the electric field, charge density and integral value of the current were calculated for both models. Air velocity distributions in the ionic wind jet were obtained and analyzed. The simulation and experiment results agree within sufficient accuracy.

Keywords: Ionic wind, Electrohydrodynamics, Corona discharge, Needle-Plane, Computer Simulation, PIV method.

1 Introduction

Ionic wind is generated by the corona discharge due to the momentum transfer from ions moving into the inter-electrode gap to neutral molecules [1]. The phenomenon underlies a number of notable modern technologies, for example, it enables the creation of silent coolers for air ventilation [2] and efficient electrostatic precipitators [1]. The devices, based on corona discharge and ionic wind, demonstrate a number of advantages over earlier types: they can function in a wide range of temperatures, produce no noise, and have no moving parts, thus providing a higher reliability.

However, the actual development of such equipment pivots on a detailed insight into the physical processes that cause ionic wind. Computer simulation of the processes requires significant computational power; therefore, different simplified models are relevant. The work aims to compare two idealized models. Simplification consisted of substitution of complicated processes in the corona sheath with a boundary condition at the active electrode. The first method utilizes an approach, when the density of the flow of positive ions is set at the active electrode as the linear function of the electric field strength. Another way of setting a boundary condition was presented in [3]. In case of the negative polarity of the high voltage electrode, it represents a setting of the variation rate of electron flow from the electrode. Work [4] adopted this option for the positive polarity case.

2 Formulation of the problem

The calculation used the finite element method in the Comsol Multiphysics software for the needleвЃ“plane electrode system with axial symmetry S (Fig.1). The distance between the electrodes is fixed ($d = 20\ mm$). The region of interest (hashed on the figure) is bounded from below by ground electrode B. Another boundary Pz separates the region of interest and outer air and is formally open. A sharp tip of anode A (needle) is considered to be spherical. The sphere radius ($0.125\ mm$) was found by using photos of real needle that had been used in the experimental part of the research.

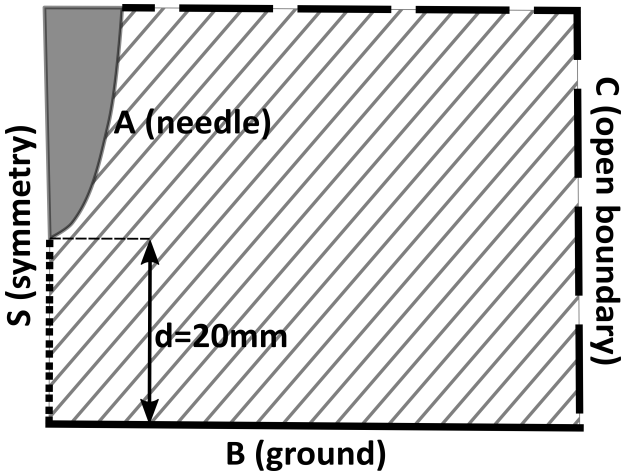

Figure 1: Schematic of the under study system

The electrohydrodynamics equation set (1) in general case describes the outer area of corona discharge, where ion-wind velocities are calculated [3]. The set includes the Poisson equation (1.1), the Nernst-вЃ“Planck equation (1.2) and NavierвЃ“Stokes equations (1.3)–(1.4), which are written in the incompressibility approximation. The interaction of ions and neutral air molecules, which sets the air in motion, is expressed by introducing the volume force $\mathbf{f} = en_i\mathbf{E}$ that appears in the right-hand part of the equation (1.3).

$$\begin{cases} \Delta\varphi = -\frac{e n_i}{\varepsilon}, \ (\mathbf{E} = -\nabla\varphi) & (1.1) \\ \frac{\partial n_i}{\partial t} + \operatorname{div}\left(n_i b\mathbf{E} - D\nabla n_i\right) = 0 & (1.2) \\ \rho\left(\frac{\partial \mathbf{V}}{\partial t} + (\mathbf{V}, \nabla)\,\mathbf{V}\right) = -\nabla p + \mu\Delta\mathbf{V} + e n_i \mathbf{E} & (1.3) \\ \operatorname{div}\mathbf{V} = 0 & (1.4) \end{cases} \tag{1}$$

Here φ is the electric potential, n_i is the ion concentration, $\mathbf{E}$ is the electric field, $\mathbf{V}$ is the air velocity, p is the pressure, e is the absolute value of the electron charge, ε is the absolute air permittivity, b is the ion mobility, D is the diffusion coefficient, ρ is the density of air, and μ is the dynamic viscosity of air. The ion mobility was chosen equal $1.9 \cdot 10^{-4}\, m^2/(V \cdot s)$, that is, within range given in [1]. The present research considers only the outer region of the corona discharge and the propagation of positive particles only (unipolar approximation). We can observe processes, which are specific to an actual corona sheath, as a result of defining the boundary condition at the active electrode. We consider two forms of the boundary condition.

In the case of first model, density of the flow of positive ions is set at the active electrode as the linear function of the electric field strength (2):

$$\mathbf{j}(E) = j_n \cdot \mathbf{e_n}, \quad j_n = \begin{cases} k \cdot (E - E_0), \ E \geq E_0 \\ 0, \ E < E_0 \end{cases}, \quad k \to \infty \tag{2}$$

In order to define this function we have to determine the value E_0, the electric field strength, at which the corona discharge ignites (the threshold field). To this end, the ignition voltage of corona discharge in the experimental electrode system was first determined by approximation of the current-voltage characteristics found experimentally. Then, computer simulation was used to tackle the auxiliary electrostatic problem (1.1) with the ignition voltage applied to the system, disregarding the space charge. The maximum value of the electric field strength that was observed at the needle was further used as E_0. Parameter k, which defines the slope of the function (2), has an evident effect on the solution of the problem. In this work, we hypothesized that the solution would attain a certain steady state with growing k. In this case, the electric field strength at the needle surface will be close to the threshold field strength E_0, at which the ionization processes start, in accordance with the general principles used in various simplified models of the corona discharge [5].

The second method that was examined in the work utilizes a more complicated boundary condition for the ion flux, which bases on calculating the number of ionization collisions near the electrode surface (3). The advantage of the model is that it requires no experimental input data at a change of the electrode configuration if the photoionization coefficient is known. If unknown, the coefficient can be measured for the electrode once in an experiment. As [2] shows, further variations of the geometrical parameters of the system require no additional experimental data for computer simulation.

$$\begin{cases} \dfrac{\partial}{\partial t} j = j \dfrac{\text{Ø} e^{M} - 1}{\text{ø}} & (3.1) \\ \text{ø} = \text{Ø} e^{M} \displaystyle\int_{0}^{b} \frac{ds}{\bar{}_{e} E\left(s\right)} & (3.2) \\ M = \displaystyle\int_{0}^{b} \text{ff}\left(E\left(s\right)\right) ds & (3.3) \end{cases} \tag{3}$$

Here j is the current density, the Ø is photoionization coefficient, $\bar{}_{e}$ is the mobility of electrons, M is the number of ionizing collisions. The variable of integration in (3.2)–(3.3) is the coordinate along electric-field line, and limits 0 and b correspond to electrode surface and the outer boundary of corona region, respectively. Function $\text{ff}(E)$ is the ionization coefficient. This research uses ff from [2]:

$$\text{ff}\left(E\right) = \begin{cases} 6.54e5\,[1/m] \cdot \bar{}_{e} E \cdot exp\left(-193e5\,[V/m]/E\right), E < 151.2e5\,[V/m] \\ 1.14e6\,[1/m] \cdot \bar{}_{e} E \cdot exp\left(-277e5\,[V/m]/E\right), E \geq 151.2e5\,[V/m] \end{cases} \tag{4}$$

Other boundary conditions are the same for both models. The full set is given in the table:

		High voltage electrode A	Symmetry axis S	Grounded electrode B	Open boundary C
both models	φ	$' = U$	$(\mathbf{E}, \mathbf{e_r}) = 0$	$' = 0$	$(\mathbf{E}, \mathbf{n}) = 0$
	$\mathbf{V}$	$\mathbf{V} = \mathbf{0}$	$(\mathbf{V}, \mathbf{e_r}) = 0$	$\mathbf{V} = \mathbf{0}$	$p{=}0$
model No2	M	–	–	$M{=}0$	–
model No1	n_i	$j = (E - E_0)$	$(\mathbf{j}, \mathbf{e_r}) = 0$	$(\nabla n_i, \mathbf{n}) = 0$	$(\mathbf{j}, \mathbf{n}) = 0$
model No2		$\frac{\partial}{\partial t} j = j \frac{\text{Ø} e^{M} - 1}{\text{ø}}$			

3 Experimental study

Verification of computer models is conducted as a comparison of calculated variable distributions to experimental data. Experimentally measured values are the electrode system current and the airflow velocity distribution. Current measurement is actually the voltage measurement on a known resistance using an ADC. The particle image velocimetry (PIV) method is used to visualize the flows in the presence of ionic wind: visualizing aerosol is sprayed in the air, its particles are illuminated with a laser beam, which goes through a cylindrical lens in order to form a lighted plane. The electrode system under study is placed in this plane in such a way that the plane is aligned with the region of interest and passes through the axis of the needle. Two shots are taken with a high-speed camera. The pair of frames show images of aerosol particle positions with a known time interval. Most probable displacements are determined using cross-correlation function. With displacements and time interval, velocity distribution is restored. In order to obtain reliable and authentic

results, multiple frame pairs are taken, and the velocities are averaged. The method reliability and absence of particles injection influence are proven in [7]. It should be noted that the laser plane is approximately *1 mm* thick, which is much greater than the radius of curvature for high-voltage electrodes used in the study. This should be taken into account, when comparing experiment and simulation results, especially if the region of the greatest velocity gradient is of the same scale.

4 Analysis of results

Below is the comparison of calculations (for both models) and experimental results. Additionally, some dependences and distributions are illustrated by the data obtained from the simulation.
The I-V curves (Fig.2 (left)) display a parabolic plot shape, typical for corona discharge. Besides, the fact follows from linearity of reduced I-V curves (current-voltage characteristics divided by voltage) shown on Fig.2 (right). The results of both models agree with the experimental curve within sufficient accuracy (about 5%). The first model describes the ignition voltage accurately, because the ignition voltage of corona discharge is a part of determined conditions for the model. But the second one predicts the threshold voltage with high accuracy also and requires no experimental I-V curve.

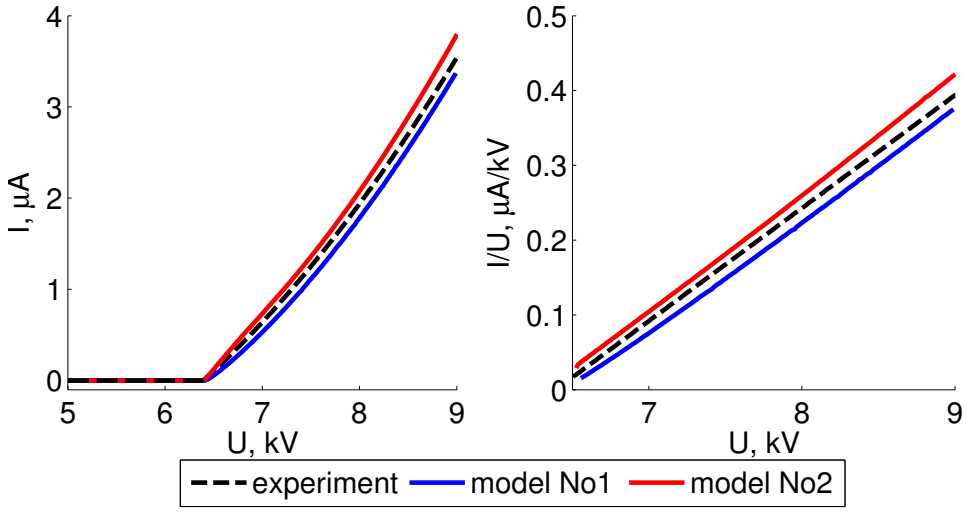

Figure 2: Current per voltage for the simulation and the experiment

The computer simulation allows finding many different quantities that we cannot measure experimentally. Fig.3 (left) shows distributions of electric field strength and ion concentration near the needle tip for voltage *8.8 kV* (the corona discharge has already ignited for the voltage). It is hard to see any visual difference in the distributions for two models, so the results only for first model are shown on the figure. The surface plots demonstrate the characteristic corona discharge distributions: the electric field attains the maximum on electrode surface and dramatically decreases with growing distance from the needle tip; the ion concentration Fig.3 (right) has

the same maximum point, but ions form a cloud that slowly spreads away from the needle tip.

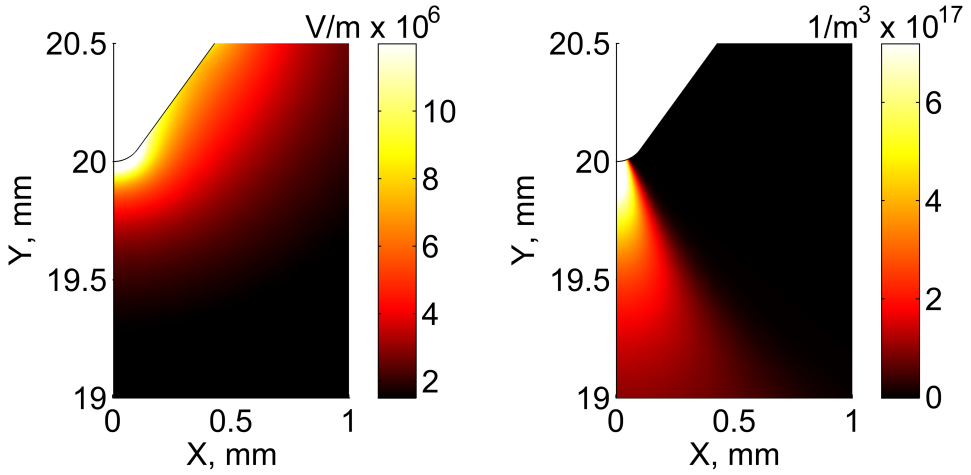

Figure 3: Distributions of electric field strength and ionic concentration in the region of needle tip

Let us consider the distribution of the electric field strength at the needle tip (Fig.4 (left), the zero point of arc length in the plot corresponds to the centerline of the system). Even though the surface field for the first method is stronger than for the second one, the total current from the electrode is higher for the second model (it is shown in I-V curve at Fig.2).The cause is that the first method uses the boundary condition, which leads to the current start only from the part of the electrode, where the electric field strength is higher than the threshold field (E_0). In the case of the second model, the produced current is independent of E_0 and is defined by the number of ionizing collisions (variable M in (3)). The needle tip distribution of M is shown on Fig.4 (right) and it is clear that the distribution shape follows that of the electric field. The relationship between these variables results from definition of M and form of function $ff(E)$ (4). Consequently, the current in the case of the second model depends also on electric field on the active electrode, but the dependence is more complicated than in the case of the first one.
The plot of axisymmetric distribution of electric field (Fig.5 (left)) illustrates the fact that the above-mentioned difference between models holds only for a small region near the needle tip. Both models yield the same values at distances more than $0.5\ mm$ from the needle (when the interelectrode gap is $20\ mm$).
The electric field maxima that correspond to different applied voltages are shown on Fig.5 (right). The plot illustrates that the difference between methods remains for every considered voltage that is higher than the ignition one. For small voltages, the plots are linear for both models, which is explained by space charge deficiency. After corona discharge ignition, electric field for both models tends to the stationary level and the second method allows predicting its value (E_0 in terms of the first one).
The velocity distributions were obtained from the simulation following the electric characteristics. Fig.6 shows the comparison between surface velocity plots for the experiment and the simulation near the symmetry axis for voltage $8.8\ kV$. It is hard to see any visual difference in the distributions for two models, so the figure

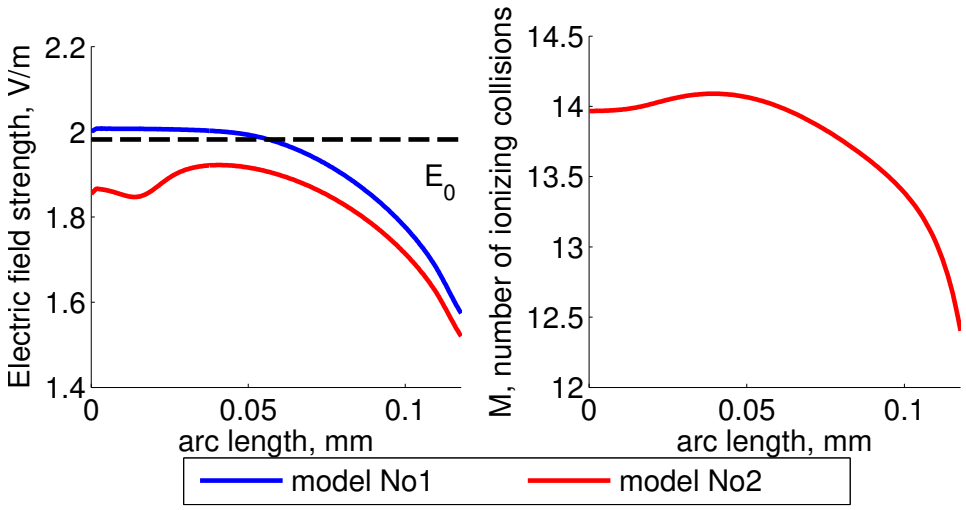

Figure 4: Electric field strength and number of ionizing collisions on the needle tip

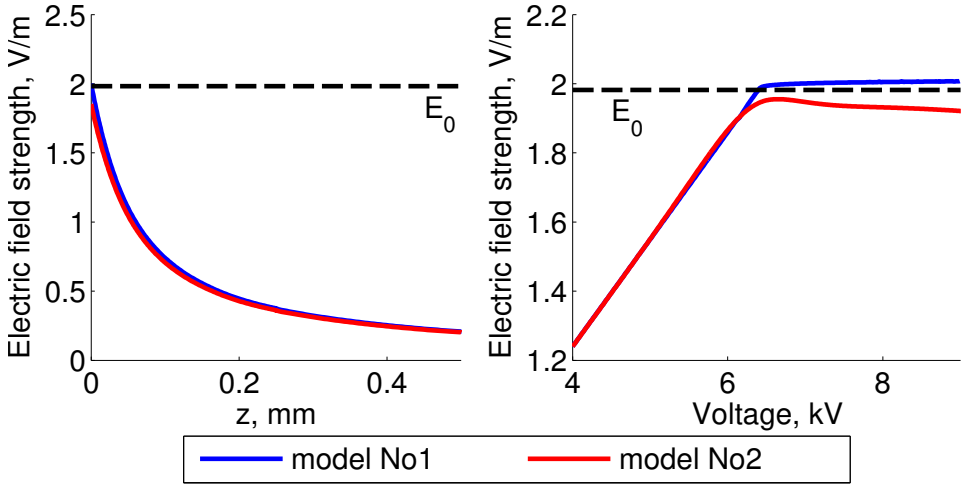

Figure 5: Axial distribution of electric field and electric field maximum from voltage

shows the results only for the first of them. Notice that the simulation gives us the structure of the jet similar to the experimental one (the scales are chosen identical and velocity maxima at right-hand plot are not shown). We can obtain more detailed information from the analysis of the line velocity plots.

The plot of radial velocity distribution for the distance of $5\ mm$ from the needle Fig.7 (left) illustrates a good agreement between models and the experiment in region $r > 0.8\ mm$. There is a singularity in the experimental research for the needle-plane system near the symmetry axis: the laser plane is about $1\ mm$ thick, and steep velocity gradient becomes smoothed. For this reason, we observe the average velocities in that region; additionally, a slight jet oscillation increases that effect. Therefore, it is not correct to compare results with the experiment for $r < 0.8\ mm$. Let us consider the vertical velocity distribution for $r = 0.8\ mm$ (Fig.7 (right)). It allows comparing the flow structures for the simulation and the experiment: they are agree within good accuracy. This means the simulation predicts the jet structure,

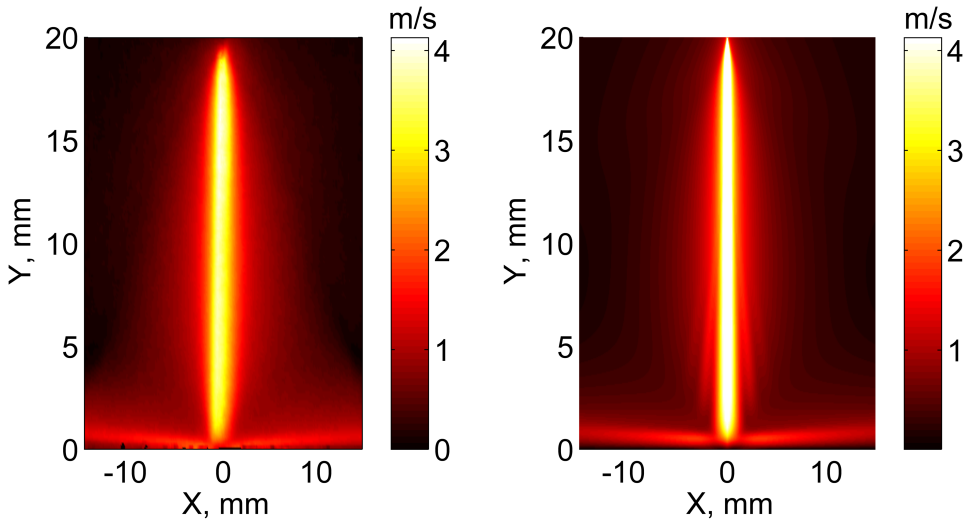

Figure 6: Velocity distributions experiment and simulation

typical for ionic wind: $0 - 3\ mm$ is the acceleration region, $3 - 17\ mm$ is the region of jet formation and $17 - 20\ mm$ is the deceleration region.

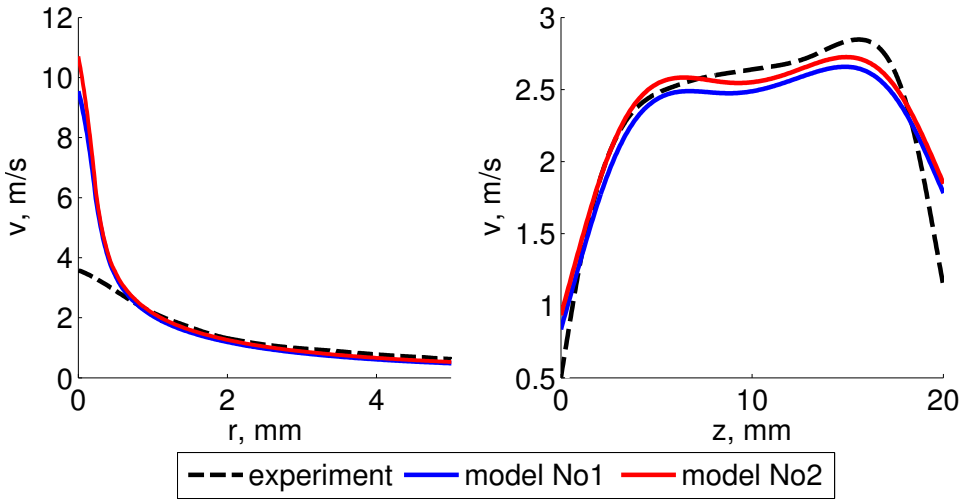

Figure 7: Radial ($5\ mm$ from needle tip) and vertical ($0.8\ mm$ from axis) velocity distributions

5 Conclusion

The computer simulation of a positive corona discharge in the needleвГYplane electrode system has been carried out. The results for ionic wind in unipolar approximation with the two types of boundary conditions on the ion flow were compared with those of experimental research. The analysis shows that the use of these types of boundary conditions allows describing the phenomenon of ionic wind within acceptable accuracy. Both methods describe special aspects of the phenomenon such as typical I-V curve and air velocity distribution.

Distributions of electric field strength, space charge density, and current on the active electrode surface demonstrate the coherence in investigated models. It should be noted that the second method is more flexible and comprehensive than the first one. This is grounded on a thorough understanding of corona discharge and generation of ionic wind. Thus, the model, based on calculation of the number of ionizing collisions, makes it possible to determine electric field strength associated with corona discharge ignition without experimental data. This fact is an advantage of the second model.
In addition, we were able to find hard-to-detect physical quantities by use of computer simulation because of similarities with the global experimental I-V curve. The knowledge of current distribution in corona discharge, distribution of electric field, ion concentration in the electrode gap, velocity of particles gives us an insight into ionic wind.

6 Acknowledgements

The study was supported financially by the Russian Foundation for Basic Research (project no. 15–08–07628a) and was performed using the equipment of resource centers вҐЁGeomodelвҐ№ and вҐЁComputing centerвҐ№ of the scientific park of the St. Petersburg State University.

References

[1] Vereshchagin I.P., Koronnyi razryad v apparatakh elektronno-ionnoi tekhnologii (Corona Discharge in Electron-Ion Devices), Moscow: Energoatomizdat, 1985.

[2] Yang F., Jewell-Larsen N.E., Brown D.L., Pendergrass K., et al., in Proc. Int. Symp. on High Voltage Engineering, Delft, Netherlands, August 25вҐY-29, 2003, pp. 1вҐY-4.

[3] Zhidkova P.S., Samusenko A.V., A computer model of the ionic wind in the unipolar approximation with the boundary condition on the ion flow variation rate, Surface Engineering and Applied Electrochemistry, 2016, 52(4), pp. 370-вҐY379.

[4] Samusenko A.V., Safronova I.F.,Stishkov Yu.K., Unipolar model of the positive corona discharge, Surface Engineering and Applied Electrochemistry, 2016, 52(5), pp. 43-вҐY50.

[5] Dordizadeh P., Adamiak K., Castle G.S.P., Parametric study of the characteristics of trichel pulses in the needle-plane negative corona discharge in atmospheric air, Journal of Electrostatics, 2016, 84, pp. 73–80.

[6] Raizer Yu.P., Fizika gazovogo razryada (Physics of Gas Discharge), Dolgoprudnyi: Intellekt, 2009.

[7] Hamdi M., Havet M., Rouaud O., Tarlet D., Comparison of different tracers for PIV measurements in EHD airflow, Experiments in Fluids, 2014, 55(4).

Kostin P.A., Poluektova K.D., Elagin I.A., Markovskii P.Y., St. Petersburg State University 7/9 Universitetskaya nab., St. Petersburg, 199034 Russia.